EXPERIMENTAL STUDY OF EXTRUSION AND SURFACE TREATMENT OF ORGANO CLAY WITH PET NANOCOMPOSITES

Karnik Tarverdi, Somchoke Sontikaew
Wolfson Centre for Materials Processing
School of Engineering and Design
Brunel University, United Kingdom

Abstract

The use of organoclay in polymers is expected to increase annually by about 5 percent. This paper describes melt blending techniques using PET nanocomposites containing commercially available organoclays with different percentage of surfactant coatings. This paper will also evaluate the morphology and mechanical properties of the composites using a range of techniques like, scanning electron microscopy, melt rheology and thermal analysis. Comparisons will be made between properties of amorphous and semi crystalline films in terms of surfactant used and material properties. It will be demonstrated that the quantity of surfactant used with the organoclays can significantly affect dispersion and properties of composites produced.

Introduction

Since Toyota successfully developed Nylon 6/organoclay nanocomposite in 1986 [1], there have been many reports in the field of the organoclay nanocomposites with different polymer systems, such as, nylon 11 and 12, nylon-66, polypropylene, polystyrene, polyethylene, Poly(vinyl chloride) and other polymeric materials. It is over a decade that the PET/organoclay nanocomposites have been studied along with its morphology, its use in packaging as gas barrier, thermal and mechanical properties have also been extensively investigated [2,3]. Generally, the PET/organoclay nanocomposites have been prepared by three different methods: in situ polymerization [4], melt blending [5], and solvent blending [6]. An important target has been to exfoliate the clay uniformly throughout the polymer matrix into individual layers of clay, and hoping that the mixing techniques used will fully exfoliate clay in PET nanocomposites and in the process it might greatly improved mechanical, thermal and gas barrier properties. Recently, Urko et al. [7] investigated the amount of surfactant necessary to use on the nanostructure by dispersing two commercial organoclays, Cloisite 15A (15A) and Cloisite 20A (20A), in the PET. Both organoclays have the same surfactant i.e. dimethyl, dehydrogenated tallow, quaternary ammonium (2M2HT) but the content of surfactant in 20A was less. The surfactant has two long alkyl groups (dehydrogenated tallow), which possibly reduces interaction between clay and the polymer chains. XRD results of this study show that the PET chains intercalate more easily into the clay layers of 20A than that of 15A due to the decrease in number of non polar groups, resulting in an increase of interaction between the matrix and the clay.

The commercial organoclays, Cloisite 10A (10A) and Nanofil-2 (N2) are also coated with the same surfactant, dimethyl, benzyl, hydrogenated tallow, quaternary ammonium (2MBHT), but the percentage of surfactant in N2 is less than in 10A. While the surfactant of 15A and 20A has two long alky tails, the surfactant of 10A and N2 has one long alkyl tail (hydrogenated tallow). And with one long alky tail in the surfactant, the polymer molecules more easily enter the clay gallery. The interlayer distance between clay layers of 10A is larger than that of N2, 1.92 nm for the former and 1.8 nm for the latter, and subsequently 10A could be more dispersed in PET than N2. However, 10A is probably more degraded than N2 at high processing temperature due to higher content of modifier, causing reduction of dispersion of clay in the PET matrix. The reduction of modifier concentration in N2 possibly increases the PET/clay interface and reduces degradation, resulting in the improvement of clay dispersion and tensile properties.

This work aims to disperse 10A and N2 in PET in order to study the effect of using different concentrations of modifier on the morphology, rheology, and tensile properties, including the effects of varying melt temperature in the range of 255-280°C.

Experimental procedure

The PET with an intrinsic viscosity of 0.5665 dl/g was kindly supplied by Wellman International Ltd., Ireland. Two different organoclays were used, Nanofil-2 kindly supplied by Süd-Chemie, Germany and Cloisite 10A from Southern Clay Products, USA. Both clays were coated with quaternary ammonium, dimethyl, benzyl, hydrogenated tallow (2MBHT), with different concentration. N2 with CEC of 75meq/100g with the interlayer distance of 1.8 nm, while 10A with CEC of 125 meq/100g with the interlayer distance of 1.92 nm. The organoclays and PET were dried at 80°C and at 140°C respectively in an oven for 24 hours. PET was blended with 2.5 wt% of organoclay in co-rotating intermeshing 40mm

diameter twin screw extruder and the modular screws were assembled with a semi severe screw profile and a devolotalisation zone three quarters down stream, with barrel temperatures of 240, 245, 250, 255, 260, 265 °C, from the hopper to the die. The extruder was operated at screw speed of 350 rpm. The PET compound was extruded through a 6 mm die and pelletized.

Tensile specimens were obtained by compression moulding. The PET granules were heated to a desired melting temperature and kept at this temperature for 2 minutes. After that, the melt was pressed for 3 minutes to get uniform thickness of about 0.15 mm. Amorphous samples were obtained by rapidly quenching the molten films. And to attain semicrystalline films, the molten films were cooled to desired crystallization temperature with cooling rate of 40°C/min and maintained at this temperature for 10 minutes.

The dispersion of the layered silicate in PET was observed using a scanning electron microscope (SEM), ZEISS's SUPRA 35VP. Surfaces were etched under vacuum in oxygen plasma for 8 minutes at 50 watts. The plasma etched samples were coated with gold before SEM. This treatment removed small amount of top surface layers of the polymer sample. Subsequently the 3-D dispersion of clay particles in the PET nanocomposite was clearly revealed.

Rheology properties were examined by using an ARES rheometer with 25 mm parallel plate geometry. Dynamic frequency sweep tests were performed in the frequency range of 0.1 to 500 rad/s with strain amplitude of 8% and at 270 °C under nitrogen.

Thermo gravimetric analysis (TGA) results were performed under nitrogen flow of 50 mL/min by using a TA Instrument (TA500) to examine the thermal stability of the organoclays. All samples were heated up to 800°C at a heating rate of 20 °C/min.

Extent of crystallinity in the samples was determined by using a differential scanning calorimetry, TA instrument DSC Q1000. Samples were encapsulated in aluminium pans and placed in a DSC cell and heated to 300°C at a ramp rate of 10°C/min under nitrogen atmosphere. The percentage crystallinity (X_c) for PET and PET nanocomposites were calculated from the following equation:

$$X_c(wt\%) = 100\frac{\Delta H_m - |\Delta H_c|}{\Delta H_m^0}$$

where ΔH_m^0 of 136 J/g is the heat of fusion of a 100% crystalline PET [8].

Dog-bone shaped samples for tensile testing were cut from the compression moulded films. The dimensions of the specimens were, gauge length 25 mm, width 4 mm and thickness 0.15 mm. The cross head speed of the tensile tester was set at 5 cm/min. The tests were carried out in an air conditioned room set at 23°C and relative humidity of 43%.

Results and discussion

In this study the morphology of the nanocomposites were observed at the fracture and also non fracture flat surfaces of the composite using SEM technique in order to identify the dispersion of the nanocomposites including phase separation with intercalation and/or exfoliation. SEM micrographs of sectioned films of the PET nanocomposites containing 2.5 wt% 10A (PET-25-10A-HS) are shown in figure 1. The nanoclay particles are clearly observed from the treated surfaces. The low magnification image in figure 1a reveals that the nanoclay particles are finely and randomly dispersed in the matrix. At higher magnification in figure 1b the edges of clay particles emerge from the matrix. Although the numbers of the layers in any clay stacks cannot be counted, the thickness of the clay stacks are in nanoscale, less than 100 nm. Figure 2 shows the morphology of the flat non fractured surfaces of the nanocomposites as in figure 1 and it reveals the surface areas of clays rather than the clay edges. With low magnification image, figure 2a, the small and large particles of clay are dispersed throughout the matrix and in figure 2b with higher magnification, some of the clay stacks are completely broken down into small stacks. However, these dispersed particles do not connect together to form a single area or a network because the number of particles are not high enough to develop networks of nanoclay. The combination of fracture and flat surface images indicates that PET-25-10A-HS exhibits a mixture of intercalated and partially exfoliated structure without the formation of the network structure of nanoclay particles. The morphology of the PET nanocomposites containing 2.5 wt% N2 (PET-25-N2-HS) in figures 3 and 4 was observed on the cross section and flat surface by using SEM respectively. From the SEM images of the flat surfaces, PET-25-N2-HS displayed larger and greater number of aggregates of clay than PET-25-10A-HS. These results indicate that it was possible to disperse Cloisite 10A in the PET matrix more than Nanofil 2 because the former has higher hydrophobicity, resulting from high content of the modifier.

TGA results of 10A and N2 in figure 5 exhibit similar patterns because both organoclays are MMT clay modified with identical modifiers but modifier concentration with N2 is lower than that used with 10A and therefore N2 has more final residue of clay than 10A. Neither of the organoclays seem to be very suitable for producing high quality PET nanocomposites because the onset decomposition temperature of 10A and N2 (200°C) is

lower than PET melt processing which is in the range of 255 to 280°C. However, weight loss of N2 at 260°C is 10% while that of 10A is 15% and therefore the thermal stability of N2 is much better than that of 10A.

Rheology of PET/organoclay nanocomposites was studied using linear viscoelastic measurements in oscillatory shear mode to examine the structure of the composites.

Figure 6 illustrates the storage modulus (G') of virgin PET (VPET), extruded PET (ExPET) and nanocomposite samples. In general, the high dispersion of the clay provides large areas of clay layers strongly interacting with the polymer chains, resulting in the increase of G' especially at low frequencies [9]. PET-25-10A-HS exhibits higher G' than PET-25-N2-HS in the low frequency range. This result shows that the dispersion of 10A is better than that of N2. It means that 10A is more compatible with PET than N2 because higher concentraton of surfactant was used.

The tensile properties in the amorphous state of VPET, ExPET and PET nanocomposites containing two different organoclays were studied and the results of tensile modulus and tensile strength are presented in figures 7a and 7b. In order to study the effect of processing temperature on mechanical properties, the film specimens were prepared by compression moulding at two different melt temperatures of 255°C and 280°C and then rapidly quenched to obtain the amorphous films. The result indicate that melt temperature does not affect tensile modulus and strength of the unfilled and filled PET with amorphous structure. Compared with VPET, the modulus is increased by 18% for PET-25-10A-HS and by 13% for PET-25-N2-HS. In figure 7b, the filled PET with 10A shows higher tensile strength than the filled polymer with N2 although both nanocomposites exhibit decrease in strength in relation to the virgin PET. But by comparison with the extruded PET, both nanocomposites enhance tensile strength. The improvement in tensile modulus confirms the SEM results that the degree of dispersion for the 10A is greater than N2 in the PET matrix.

In this work the effect of melt temperature on mechanical properties of semicrystalline PET and PET nanocomposites were also studied. Figure 8 shows tensile modulus and strength at different melt temperatures of 255, 260, 270 and 280°C. The tensile modulus of all samples, in figure 8a, is not affected by the melt temperature. The tensile moduli are enhanced by 24% for the semicrystalline PET-25-10A-HS and 21% for the semicrystalline PET-25-N2-HS relative to VPET. In contrast, the tensile strength of both semicrystalline nanocomposites decreases with increasing melt temperature compared with VPET as well as ExPET. Interestingly, the tensile strength of the semicrystalline nanocomposites based on N2 exhibits significantly higher tensile strength than that of the samples with 10A, especially at the processing temperature of 255-260°C. This is because of the degradation of the modifier in the organoclays at temperatures higher than 200°C, resulting in broken PET chains. According to the TGA result, N2 is more stable than 10A at PET processing temperature. For this reason the tensile strength of semicrystalline PET with 10A was poorer than that of PET with N2 for all melt temperature.

Conclusions

It was found that the amount of surfactant in the organoclay significantly affects nanoclay dispersion and consequently the tensile properties. Increase of surfactant content from 75 meq/100g for N2 and 125 meq/100g for 10A leads to greater degree of clay dispersion and higher tensile modulus, in agreement with the melt rheology results. For the amorphous films, the tensile modulus and strength increased with the increase of surfactant but the results were not affected by changing the processing temperature. But for semicrystalline films, the tensile strength decreased when the processing temperature was increased mostly due to degradation of the surfactant, especially with the samples containing higher percentage of surfactant.

Acknowledgements

The authors would like to acknowledge The Thai Government, EU FlexiFunBar Framework 6 Programme for funding this work.

References

1. O. A., and U. A., *Mater. Sci. Eng.* ***C*** **3**, 109 (1995)
2. Y. Ke, C. Long, and Z. Qi, *J. Appl. Polym. Sci.*, **71**, 1139 (1999)
3. J. C. Matayabas, and S. R. Turner. In *Polymer-Clay Nanocomposites*; T.J. Pinnavaia, G. W. B., Ed.; Wiley: New York, 2001.
4. S. H. Kim, and S. C. Kim, *J. Appl. Polym. Sci.*, **103**, 1262 (2007)
5. C. H. Davis, L. J. Mathias, J. W. Gilman, D. A. Schiraldi, J. R. Shields, P. Trulove, T. E. Sutto, and H. C. Delong, *J. Polym. Sci. Part B: Polym. Phys.*, **40**, 2661 (2002)
6. C. F. Ou, M. T. Ho, and J. R. Lin, *J. Appl. Polym. Sci.*, 91, **140** (2004)
7. U. Gurmendi, J. I. Eguiazabal, and J. Nazabal, *Macromol. Mater. Eng*, 292, **169** (2007)
8. H. W. Starkweather, P. Zoller, and G. A. Jones, *J. Polym. Sci. Polym. Phys.*, **21**, 295 (1983)
9. R. Krishnamoorti, and K. Yurekli, *Current Opinion in Colloid & Interface Science*, **6**, 464 (2001)

Key Words

Recycling, PET, extrusion, nanocomposites, polymer modifications

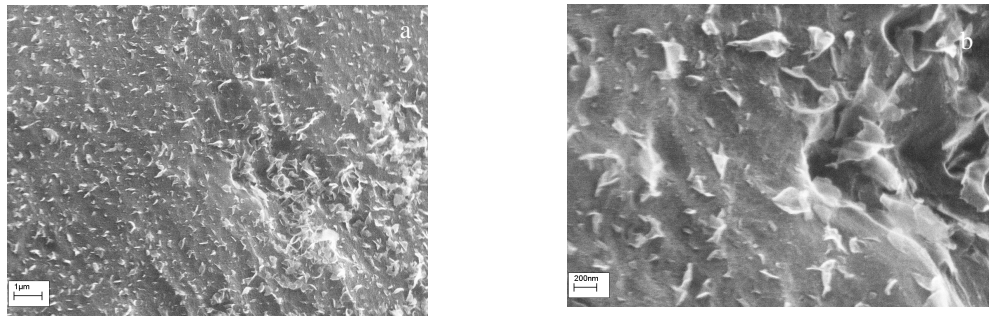

Figure 1 SEM images of cross-section of PET-25-10A-HS at (a) low and (b) high magnification

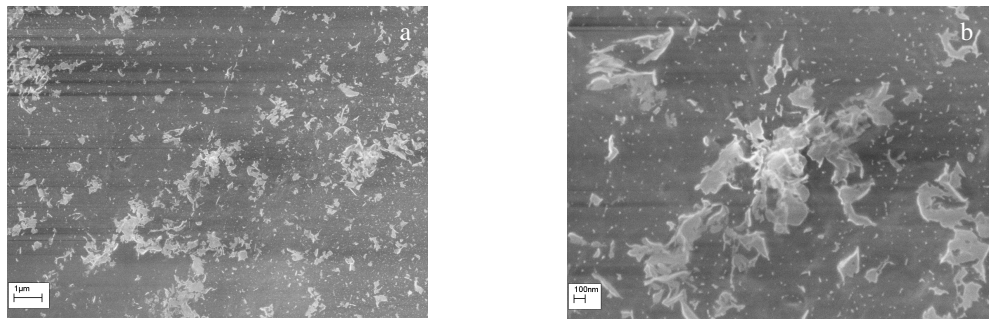

Figure 2 SEM images of surfaces of PET-25-10A-HS at (a) low and (b) high magnification

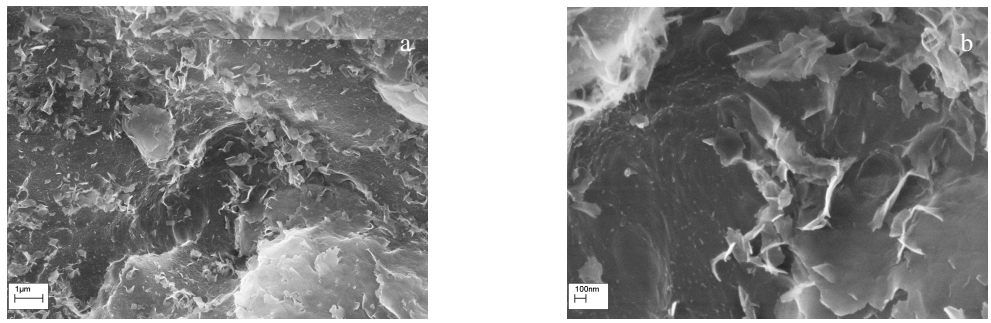

Figure 3 SEM images of cross-section of PET-25-N2-HS at (a) low and (b) high magnification

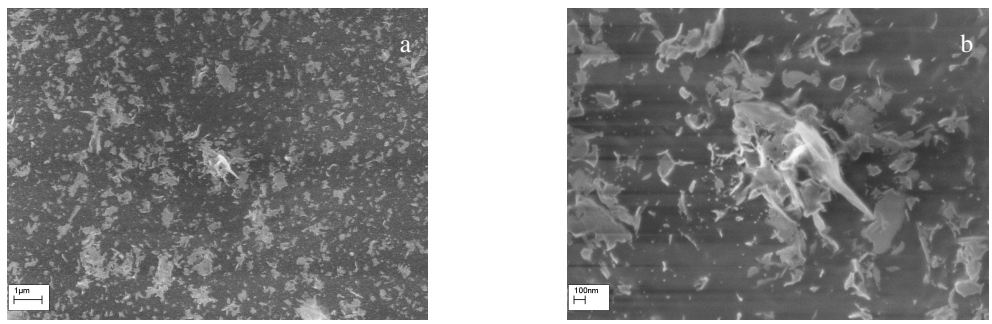

Figure 4 SEM images of surfaces of PET-25-N2-HS at (a) low and (b) high magnification

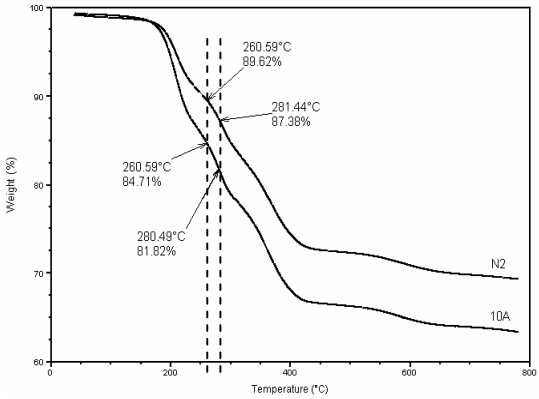

Figure 5 TGA results of 10A and N2

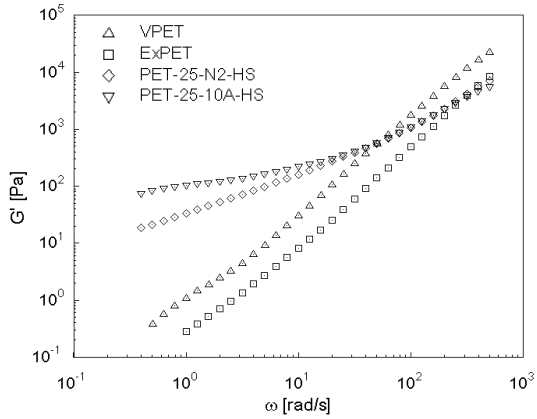

Figure 6 G′ of VPET, ExPET and composites

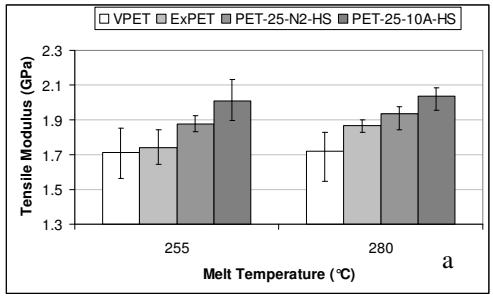

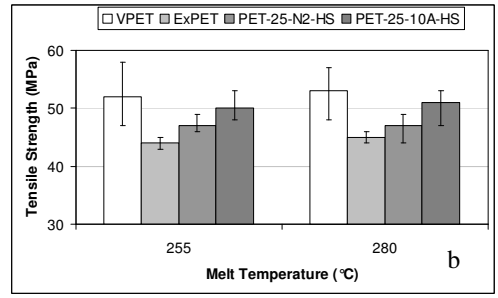

Figure 7 (a) Tensile modulus (b) Tensile strength for amorphous films of VPET, ExPET and PET nanocomposites

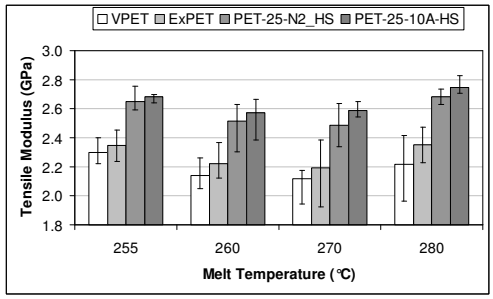

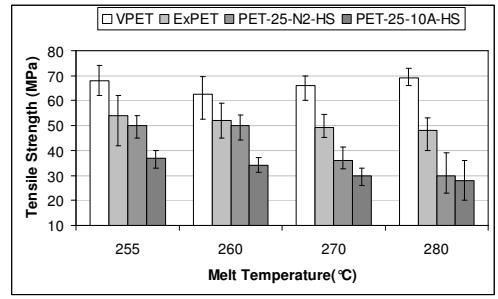

Figure 8 (a) Tensile modulus, (b) Tensile strength for semicrystalline PET and PET nanocomposite films (After compression moulding, crystallisation controlled at 200°C for 10 minutes)